ACS APPLIED MATERIALS & INTERFACES

www.acsami.org

Research Article

Programming Orientation in Liquid Crystalline Elastomers Prepared with Intra-Mesogenic Supramolecular Bonds

Kristin L. Lewis,[‖] Katie M. Herbert,[‖] Valentina M. Matavulj, Jonathan D. Hoang, Eric T. Ellison, Grant E. Bauman, Jeremy A. Herman, and Timothy J. White*

Cite This: *ACS Appl. Mater. Interfaces* 2023, 15, 3467−3475

Read Online

ACCESS | Metrics & More | Article Recommendations | Supporting Information

ABSTRACT: The large, directional stimuli-response of aligned liquid crystalline elastomers (LCEs) could enable functional utility in robotics, medicine, consumer goods, and photonics. The alignment of LCEs has historically been realized via mechanical alignment of a two-stage reaction. Recent reports widely utilize chain extension reactions of liquid crystal monomers (LCM) to form LCEs that are subject to either surface-enforced or mechanical alignment. Here, we prepare LCEs that contain intra-mesogenic supramolecular bonds synthesized via direct free-radical chain transfer photopolymerization processible by a distinctive mechanical alignment mechanism. The LCEs were prepared by the polymerization of a benzoic acid monomer (11OBA), which dimerized to form a liquid crystal monomer, with a diacrylate LCM (C6M). The incorporation of the intra-mesogenic hydrogen bonds increases the achievable nematic order from mechanical programming. Accordingly, LCEs prepared with larger 11OBA concentration exhibit higher magnitude thermomechanical strain values when compared to a LCE containing only covalent bonds. These LCEs can be reprogrammed with heat to return the aligned film to the polydomain state. The LCE can then be subsequently programmed to orient in a different direction. The facile preparation of (re)programmable LCEs with supramolecular bonds opens new avenues for the implementation of these materials as shape deployable elements.

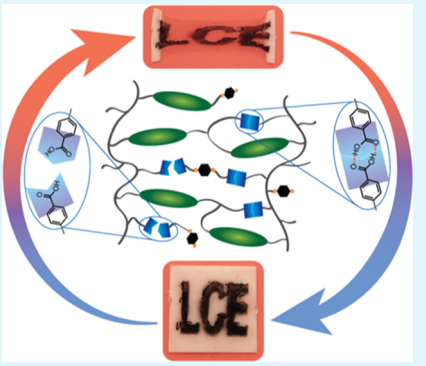

KEYWORDS: *liquid crystalline elastomers, supramolecular bonds, polymers, robotics, actuation*

INTRODUCTION

Liquid crystalline elastomers (LCEs) are widely considered for potential utility in soft robotics,[1−3] health science,[4,5] optics,[6,7] and consumer products. The retention of liquid crystallinity in LCEs is the basis for their large stimuli-response.[8−11] The retention of orientation in LCEs has been leveraged to direct cell proliferation[12−14] and as the basis for tunable optical elements.[7,15] Here, we are concerned with the thermomechanical response of LCEs. As first demonstrated by Finkelmann, aligned LCEs exhibit large directional strain (up to 75% strain) upon heating through a liquid crystalline phase transition (usually the nematic to isotropic state).[16] The temperature-dependent orientational order (referred hereafter as thermotropic) amplifies the magnitude of the response in which the material strongly contracts along the nematic director ($\hat{n}$). The alignment of LCEs, which is arrested by crosslinking, has historically been realized with mechanical alignment,[17] but recent reports widely utilize surface alignment[17] or 3D printing.[18]

The renewed interest in LCEs has been facilitated in part by the development of facile, accessible chemistries. Specifically, LCEs have been prepared by aza-Michael addition,[19] thiol-Michael addition,[17] radical photopolymerization,[20] and thiol-ene reactions.[21] The widespread adoption of these chemistries has opened up new, unexplored opportunities not accessible with classical hydrosilylation techniques.[22] Of relevance to the work presented here, we recently have introduced the utilization of chain-transfer reactions as a simple, one-pot method to prepare LCEs.[17,23−25] The short-chain, branched network resulting from chain-transfer reactions produces LCEs with low modulus and close coupling of order and temperature.[26]

A recent approach to enhance and tune thermal actuation has focused on reduction of mesogen−mesogen interactions in LCEs.[26] The stimuli response of LCEs prepared with these mesogens is comparatively sharper and shifts to lower temperatures.[26] Other reports have examined the effect of non-liquid crystalline constituents to modify crosslink density and affect interactions through pendant functional groups.[27] These investigations demonstrate the ability to tune thermomechanical properties through an understanding of molecular contributions, including spacer, crosslinker, and mesogen concentrations.[28]

Received: October 22, 2022
Accepted: December 21, 2022
Published: January 4, 2023

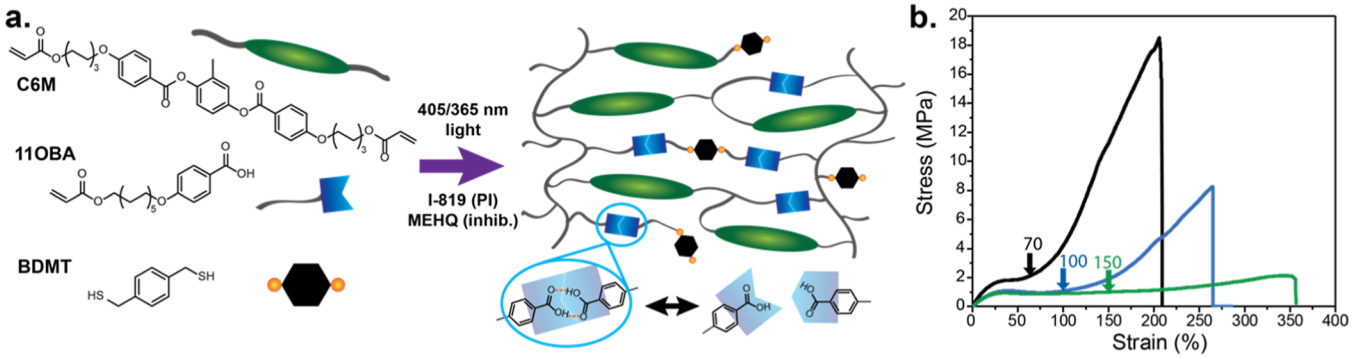

Figure 1. (a) Chemical structures of the liquid crystal monomer (C6M), monomeric form of the benzoic acid derivative (11OBA), and dithiol (BDMT). Upon polymerization, these materials form a polymer network, in which the 11OBA dimerizes to form mesogenic groups. The dithiol BDMT serves primarily as a chain transfer agent but can also act as a chain extender. (b) Tensile analysis of LCEs with increasing 11OBA concentration. The inset arrows indicate the approximate end of the soft elastic plateau. $C6M_{1.0}$ (black), $C6M_{0.8}11OBA_{0.2}$ (blue), and $C6M_{0.6}11OBA_{0.4}$ (green).

To further address this challenge, the inclusion of exchangeable bonds within LCEs has demonstrated several advantages.[29] These chemistries, such as thiourea exchange,[30] disulfide exchange,[31] and transesterification reactions,[32] can form stable networks, break under stimulus, and then reform to reinstate the integrity of the network.[29] Recent works have demonstrated the advantages of dynamic and supramolecular bonds in LCEs to facilitate programmable shapes,[33−35] healable materials,[36−38] and additive manufacturing.[39] The inclusion of hydrogen bonds as exchangeable bonds within liquid crystalline networks (LCNs) and some LCE systems has been studied previously.[40] These reports have emphasized chemical responsiveness and the dynamic response of hydrogen bonds to heat or light.[36,38,39,41−44]

This examination utilizes dimerized liquid crystalline monomers based on oxy-benzoic acid (OBA). The liquid crystallinity of OBA dimers was well-studied in low molar mass compositions by Kato and Fréchet.[45] Subsequent reports have detailed the integration of OBA dimers in glassy liquid crystalline polymer networks (LCNs).[40,41,43,46,47] However, the thermomechanical response of LCNs is limited, due to the comparatively large crosslink density that limits the extent of order disruption. Here we seek to integrate these hydrogen-bonded dimers, which prior reports detail disrupt sharply at the phase transition, in LCEs.[45] The incorporation of hydrogen bonds facilitates a distinctive method to program and reprogram director orientation in the LCE. The thermomechanical response of the OBA-containing LCEs is distinguished, with nearly a fourfold increase in strain rate when compared to a conventional LCE based entirely on covalent bonds.

RESULTS AND DISCUSSION

LCEs with intra-mesogenic supramolecular bonds were prepared using photoinitiated thiol-acrylate radical polymerization (Figure 1a). The copolymerization of certain dithiol monomers with liquid crystalline diacrylate monomers prepares LCEs with suppressed glass transition temperatures (T_g) associated with dangling chain ends (Figure 1a).[23−25] Acrylate-terminated liquid crystal mesogens 1,4-bis-[4-(6-acryloyloxyhexyloxy)benzoyloxy]-2-methylbenzene (C6M) and 4-(11-acryloylundecyloxyl) benzoic acid (11OBA) were melt-mixed (110 °C) with the dithiol (1,4-benzenedimethylthiol, BDMT), photoinitiator (I-819), and radical inhibitor (MEHQ) and polymerized to form LCEs (Figure 1a). Further details can be found in the Experimental Section. The 11OBA dimeric monomer is crystalline at room temperature, transitions to the smectic phase at 101 °C, subsequently transitions to the nematic phase at 110 °C, and transitions to the isotropic state at 112 °C (Figure S1). Upon polymerization, the LCEs retained the nematic phase with polydomain orientation and were subsequently removed from the cell. These materials were found to be environmentally stable in laboratory conditions.

This examination compares the alignment and stimuli response of three LCE formulations differentiated by the molar ratio of conventional LC mesogens (C6M) to LC dimers (11OBA). The LCE compositions are identified as $C6M_x11OBA_y$ where x is the mole fraction of C6M in the network and y is the mole fraction of 11OBA. For example, $C6M_{0.8}11OBA_{0.2}$ has a ratio of 0.8:0.2 moles C6M:11OBA, respectively. The thermotropic phase transitions of the 11OBA monomer and LCEs were determined using differential scanning calorimetry (DSC). The glass transition temperature (T_g) and the nematic to isotropic phase transition temperature (T_{NI}) of each formulation are summarized in Table 1. The corresponding DSC thermograms are provided in Figure S2. The transition peak on the DSC thermogram of the $C6M_{1.0}$ LCE is very weak and broad. This indicates that the T_{NI} of this material has a strong second-order character, likely due to the high density of covalent crosslinks. Incorporating the 11OBA dimeric mesogen into the LCE shifts the T_{NI} to 94 °C, evident in both the DSC thermograms and polarized optical micrographs (Figure S3). However, $C6M_{0.8}11OBA_{0.2}$ and $C6M_{0.6}11OBA_{0.4}$ have notable increases in the enthalpy of the transition associated with increasing 11OBA content (Table 1). The enthalpy values are indicative of both the

Table 1. Material Properties for LCEs $C6M_{1.0}$, $C6M_{0.8}11OBA_{0.2}$, $C6M_{0.6}11OBA_{0.4}$, and $11OBA_{1.0}$

LCE name	T_g (°C)	T_{NI} (°C)	enthalpy of T_{NI} (J/g)	Young's modulus (MPa)
$C6M_{1.0}$	7.1	103	0.3	8.38
$C6M_{0.8}11OBA_{0.2}$	0.3	94	1.1	4.86
$C6M_{0.6}11OBA_{0.4}$	−1.2	94	2.4	4.34
$11OBA_{1.0}$	32	120	25	N/A

https://doi.org/10.1021/acsami.2c18993
ACS Appl. Mater. Interfaces 2023, 15, 3467−3475

potential for higher order as well as the association of order disruption and the intra-mesogenic bonds.[48]

All three LCEs exhibit typical stress−strain responses, including a soft elastic plateau where the LC mesogens reorient from polydomain nematic to monodomain nematic at no stress penalty (Figure 1b). As 11OBA concentration is increased in the LCE, the Young's modulus decreases, the materials exhibit a reduced stress at break and higher strain at break, and the soft elastic plateau is lengthened (Table 1). This might be expected as the weaker hydrogen bonds yield more easily under mechanical strain (as opposed to the LCE based on purely covalent bonds). Unfortunately, the mechanochemical sensitivity of LCEs with 50 mol % or higher 11OBA concentrations would permanently deform with mechanical alignment and accordingly is not subject to the examination presented here. Comparatively, the copolymerization of 11OBA (i.e., 100 mol % 11OBA) with BDMT forms a material with a T_g above room temperature which resulted in a glassy material. This material demonstrated a broad T_{NI} with a very large enthalpy on DSC. However, because of the glassy nature and limited stimuli-response (strain), as well as extensive prior study of similar systems,[40] we did not examine this material here (Figure S1).

The incorporation of mechanochemically sensitive hydrogen bonds in the LCEs with 11OBA is a distinctive approach to mechanical alignment. LCEs were mechanically aligned after preparation (i.e., without the need of a second reaction) by simultaneously heating and stretching the films to the strain values indicated in Figure 1b. As described by the theory of Warner,[49,50] the polydomain−monodomain transition in LCEs has three regions: (i) a classical linear region, (ii) a nonlinear plateau (i.e., "soft elastic region"), and (iii) a classical strain hardening region. Notably, the soft elastic region is indicative of maximal director reorientation. Accordingly, per Figure 1b, the magnitude of the strain necessary to enforce orientation in the three materials (i.e., to reach the strain hardening region) is different. Thus, in order to align each LCE with the maximum possible alignment, the LCEs were manually stretched to 70% strain for $C6M_{1.0}$, 100% strain for $C6M_{0.8}11OBA_{0.2}$, and 150% strain for $C6M_{0.6}11OBA_{0.4}$. The LCE films in the polydomain state were heated to 90 °C, just below the T_{NI}, during mechanical alignment to facilitate the disruption of the hydrogen-bonded mesogens. This allows for further reorientation of the remaining mesogens to achieve an improved monodomain nematic state (Figure 2a). The retention of alignment is evident in polarized optical microscopy (POM) images taken at 0 and 45° relative to the nematic director (Figure S4). Wide angle X-ray scattering (WAXS) confirms the nematic phase with calculated orientation parameters (S) of 0.54 for $C6M_{1.0}$, 0.73 for $C6M_{0.8}11OBA_{0.2}$, and 0.79 for $C6M_{0.6}11OBA_{0.4}$ at room temperature. The corresponding WAXS patterns for these samples at 25 °C are presented in Figure S5. The orientation parameter of the LCE increases with increasing 11OBA content which indicates that the mechanochemistry of the supramolecular bonds is potentially contributing to the soft elastic deformation, manifested in an increase in achievable orientation parameter.

The labile hydrogen bonds of 11OBA further allow the LCE to be readily reprogrammed without the need for an additional reaction step. The reprogramming of the LCEs is similar to so-called one-way shape memory processing. Reprogramming of the LCE is visualized in Figure 2b, where an initially polydomain LCE is heated and stretched along a single axis

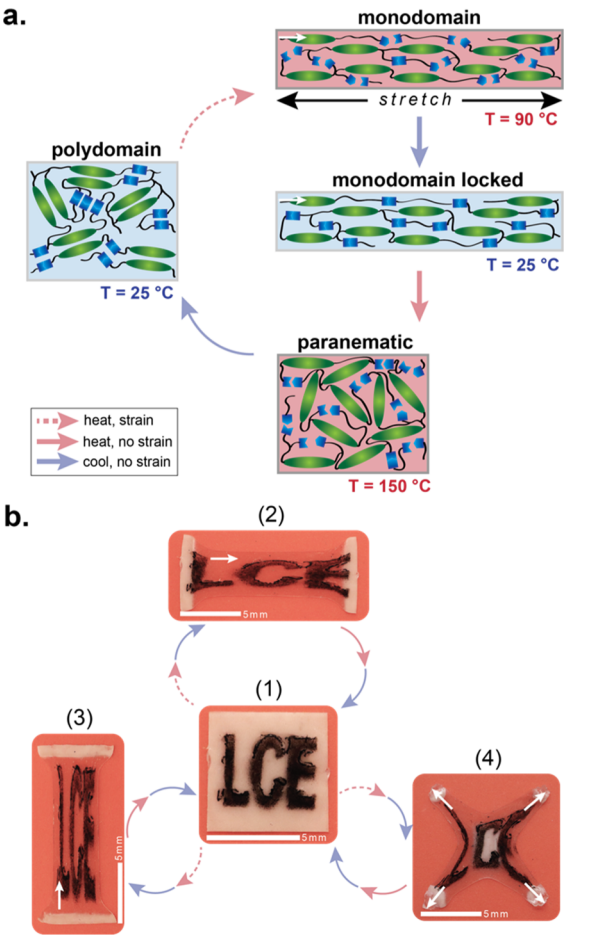

Figure 2. LCEs prepared with intra-mesogenic supramolecular bonds can be programmed and reprogrammed. Here, dashed red arrows indicate heating with load (deformation), solid red arrows indicate heating without load, and solid blue arrows denote cooling without load. (a) Illustration of the stretch alignment process to transition the initially polydomain orientation to monodomain and return via the paranematic state to the polydomain orientation. (b) Reprogramming of the $C6M_{0.6}11OBA_{0.4}$ polydomain film (1) stretched to ca. 150% strain along the x-axis (2), y-axis (3), and biaxially (4). After each axial programming, the sample is returned to (1) as per (a) before being reprogrammed along another axis. Solid white arrows indicate the direction of deformation that prescribes the nematic director after cooling.

(e.g., the x-axis). The LCE retains a monodomain orientation along the deformed axis. Upon heating the freestanding (i.e., absent of any tensile load) film above the T_{NI}, the LCE contracts due to an order−disorder response to temperature (Figure 2a). Upon cooling, the freestanding (again, absent of load) LCE returns to the polydomain state. The LCE can be reprogrammed with a load in the opposite axis (e.g., the y-axis). The LCE retains the orientation again along the deformed axis (Figure 2b). Upon a heat−cool cycle that surpasses T_{NI}, the LCE again reforms the polydomain state. The deformation of the LCEs with temperature is shown to be highly repeatable after each linear reprogramming cycle, as shown in Figure S6. The LCE can also retain complex alignment, introduced by multi-axis deformation. Here, we apply biaxial strain to the material to introduce an alignment pattern approximating a −1 topological defect (Figure 2b). Comparatively, for the LCE entirely composed of covalent

https://doi.org/10.1021/acsami.2c18993
ACS Appl. Mater. Interfaces 2023, 15, 3467−3475

mesogens (i.e., $C6M_{1.0}$ LCE), the retention of orientation is limited when subject to similar processing and reprocessing (Figure S7).[25] Thus, we conclude that the addition of intra-mesogenic hydrogen bonds enables a distinctive approach to align LCEs prepared with free-radical chain transfer photopolymerization.

The association of the mechanochemistry of the intra-mesogenic hydrogen bonds and alignment was further examined with attenuated total reflectance infrared spectroscopy (ATR-IR). Prior examination of LC dimers based on benzoic acid derivatives has utilized a temperature-dependent shift in IR from 1680 to 1730 cm^{-1} for the carbonyl peak to isolate the role of hydrogen bonding and phase behavior (Figure 3a).[45,48,51,52] The LCE composition examined here has multiple components containing carbonyl bonds that generally contribute to the vibrational mode at 1730 cm^{-1}. However, the dimeric form of OBA has a distinguished vibrational mode at 1680 cm^{-1}, which can be used to monitor the relative increase in concentration of monomeric OBA in the LCE upon heating. This is confirmed in the materials shown in Figures 3b and S8,

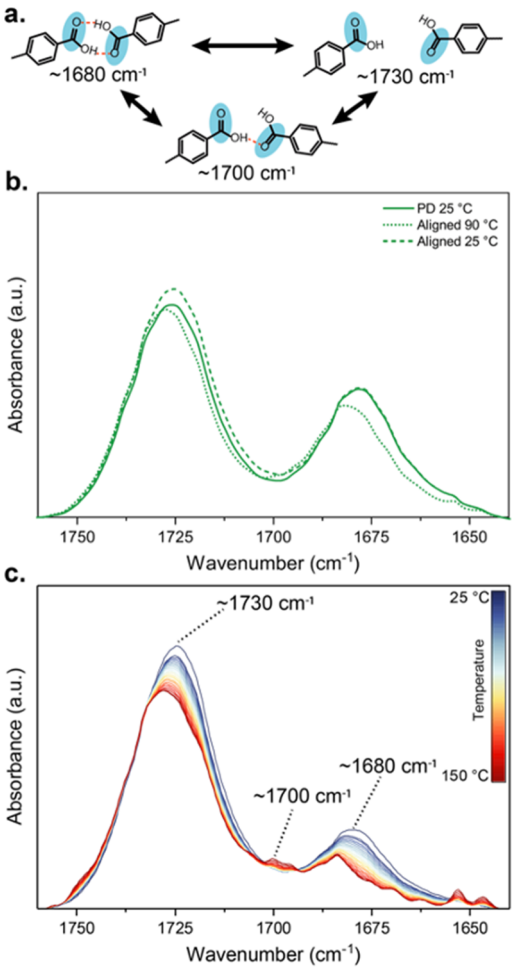

Figure 3. (a) Illustration of structural variations in H-bonding 11OBA between a dimer, open dimer, and monomer state. (b) ATR-IR spectra of the carbonyl regime for $C6M_{0.6}11OBA_{0.4}$ taken in the polydomain (PD) state at room temperature, aligned state at 90 °C, and locked aligned state at room temperature. (c) Temperature-dependent (50−150 °C) ATR-IR spectra for $C6M_{0.8}11OBA_{0.2}$ illustrating the transition from dimerized 11OBA (1680 cm^{-1}) to free 11OBA (1730 cm^{-1}).

where the 1680 cm^{-1} peak is nonexistent for the control sample ($C6M_{1.0}$) but increases in magnitude with 11OBA concentration. ATR-IR spectra were collected at 5 °C intervals from 50 to ca. 150 °C (experimental limitations did not allow us to heat beyond 150 °C). These data are presented in Figures 3c and S9. As the temperature increased, the peak at 1680 cm^{-1} decreases in intensity and shifts to higher wavenumbers, confirming a conversion of dimeric to monomeric and open dimer 11OBA units. The appearance of the carbonyl peak at 1700 cm^{-1} indicates the formation of open dimers (Figure 3a).[52]

By deconvoluting these peaks (Figure S10) and finding the area under each, the fraction of monomer species (f_{1730}) within the films as a function of temperature can be found using

$$f_{1730} = \frac{A_{1730}}{A_{1730} + A_{1680}} \quad (1)$$

where A_x corresponds to the area under a given peak.[48] Figure S11 highlights the fraction of monomer species at each temperature point for the two films containing hydrogen bonding. We assume the fraction of monomer species at room temperature is negligible, and the data were normalized accordingly. Using a reference line derived from the T_{NI} found using DSC, it is evident that the LCEs exhibit a stepwise increase in the amount of monomer present at the nematic to isotropic transition. This indicates that as temperature is increased through the T_{NI}, the supramolecular bonds become more labile and break, resulting in fewer mesogenic units and less restriction on the LCE polymer network.

Thus, the alignment process is undertaken on the materials when the H-bonds are disrupted, allowing the C6M mesogens to reorient more freely. Figures 3b and S8 demonstrate that when LCEs are stretched and heated to 90 °C, the peak at 1680 cm^{-1} decreases from its initial intensity at room temperature in the polydomain state. This shows the correlation of a higher concentration of H-bonds and increased alignment of the LCE. Upon cooling, the 11OBA segments are clearly able to reform dimeric mesogenic units, as evident in the IR spectra (Figures 3b and S8), as the programmed orientation is then effectively locked in.

The inclusion of intra-mesogen hydrogen bonds also contributes to the stimuli-response of the LCEs, which can reversibly occur when the films are held under tension. The thermomechanical response of the aligned LCEs was examined when held in tension in a DMA during heat−cool cycles initially from room temperature through the T_{NI} to 150 °C (isotropic/paranematic state) and cycled between 60 and 150 °C. The alignment and thermomechanical response measurements undertaken with the DMA are further explained in the Experimental Section. The conventional LCE $C6M_{1.0}$ exhibits a continuous deformation upon heating (Figure 4a) and cooling (Figure 4b). The introduction of 11OBA shifts the thermomechanical response to lower temperatures and sharpens the rate of strain generation. Most notably, the introduction of 11OBA increases the magnitude of strain generated, which is likely attributable to the differences in the orientation parameter of the LCE. Figure S11 illustrates the correlation between hydrogen bonds dissociating and improved actuation. The LCE with the largest concentration of 11OBA, $C6M_{0.6}11OBA_{0.4}$, demonstrates a sharp increase in the fraction of monomer at the T_{NI}, which corresponds to a

https://doi.org/10.1021/acsami.2c18993
ACS Appl. Mater. Interfaces 2023, 15, 3467−3475

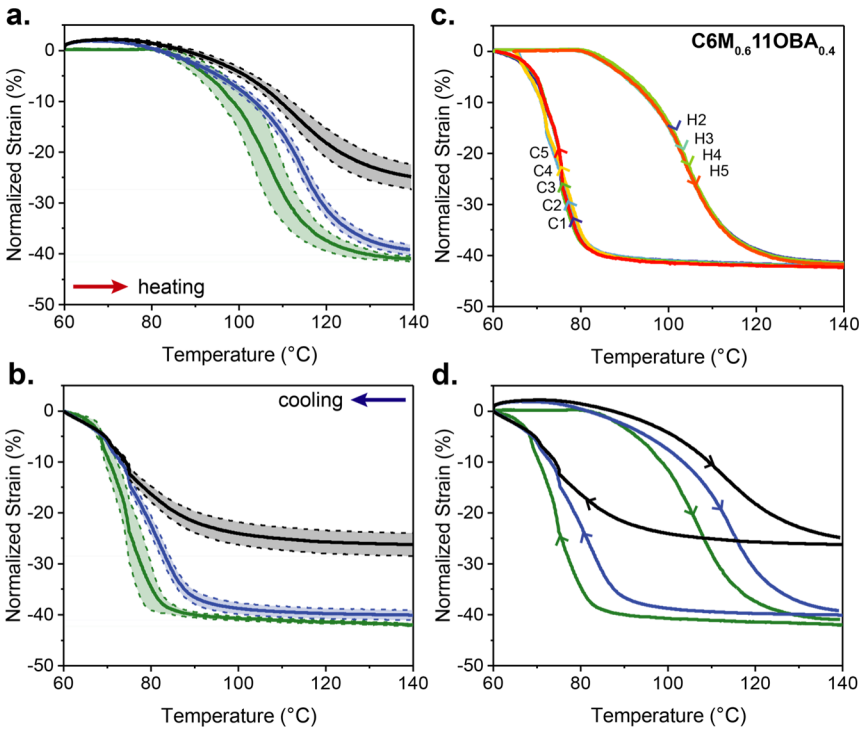

Figure 4. Thermal actuation curves illustrating change in strain for LCEs upon (a) second heating (60−140 °C; ramp rate = 5 °C min^{-1}) and (b) first cooling (140−60 °C; ramp rate = 5 °C min^{-1}). (c) 5× actuation hysteresis curves after first heating of the $C6M_{0.6}11OBA_{0.4}$ sample showing heating (H) and cooling (C) cycles. (d) Second heating and first cooling cycles for LCEs with arrows indicating the direction of temperature. $C6M_{1.0}$ (black), $C6M_{0.8}11OBA_{0.2}$ (blue), and $C6M_{0.6}11OBA_{0.4}$ (green). Shadows reflect standard deviation of multiple runs ($n \geq 3$).

more rapid actuation at a lower temperature. Evident in Figure 4a,b, but isolated in Figure 4c, is the hysteretic response of the LCE. Here, the actuation of $C6M_{0.6}11OBA_{0.4}$ is measured over five cycles. After the first heating cycle, the LCE consistently exhibits a thermomechanical response. The hysteresis is evident in all three LCE samples examined here (Figure 4d) and generally associated with the response of LCEs prepared by free-radical chain transfer photopolymerization.[23]

The incorporation of 11OBA in both $C6M_{0.8}11OBA_{0.2}$ and $C6M_{0.6}11OBA_{0.4}$ sharpens the thermomechanical actuation of the materials, as shown in Figure 5a,b, which plots the derivative of the strain−temperature curves for these materials. Comparatively, introducing 11OBA concentration increases the rate of stimuli response from −0.82 to −1.80 %ε °C^{-1} for $C6M_{0.6}11OBA_{0.4}$ (Figure 5a). The increased slope of the strain−temperature curve is consistently observed for the samples with increasing 11OBA content, even when all three samples are aligned by subjecting to an equivalent alignment strain of 35% (Figure S12). Upon cooling, the contribution of intra-mesogenic hydrogen bonding to thermomechanical response is even more pronounced where the stimuli response of the LCE prepared from $C6M_{0.6}11OBA_{0.4}$ extends at 3.11 %ε °C^{-1} (Figure 5b). Again, all three LCE samples exhibit a shift in the thermotropic actuation on cooling, which is associated with the hysteresis seen in Figure 4d. The increase in the thermomechanical response on cooling may be attributed to the large degree of disorientation of the LCE network at temperatures above the T_{NI} from the disruption of H-bonded mesogens. The network at high temperature has effectively a lower crosslink density as the H-bonds are broken such that upon cooling, the LCE can more rapidly transition to the nematic state. Thus, the stimuli response is sharpened considerably for the $C6M_{0.6}11OBA_{0.4}$ LCE.

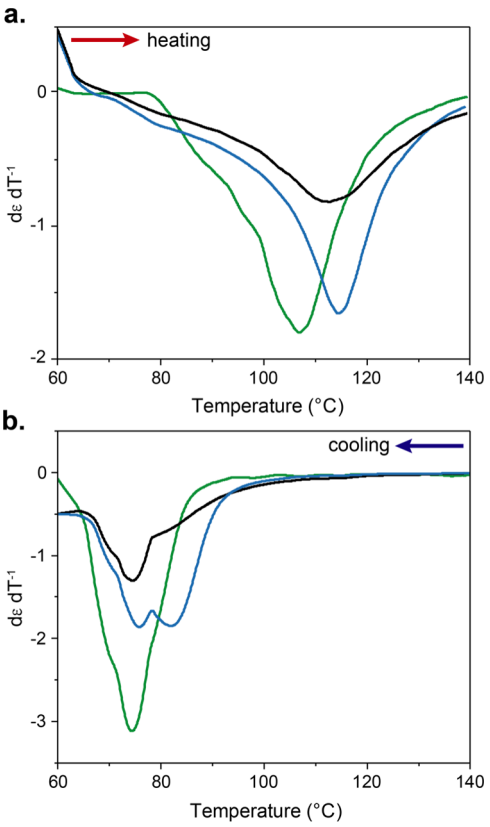

Figure 5. Derivatives of the strain−temperature curves for (a) heating and (b) cooling of the LCE samples are plotted as a function of temperature. $C6M_{1.0}$ (black), $C6M_{0.8}11OBA_{0.2}$ (blue), and $C6M_{0.6}11OBA_{0.4}$ (green).

https://doi.org/10.1021/acsami.2c18993
ACS Appl. Mater. Interfaces 2023, 15, 3467−3475

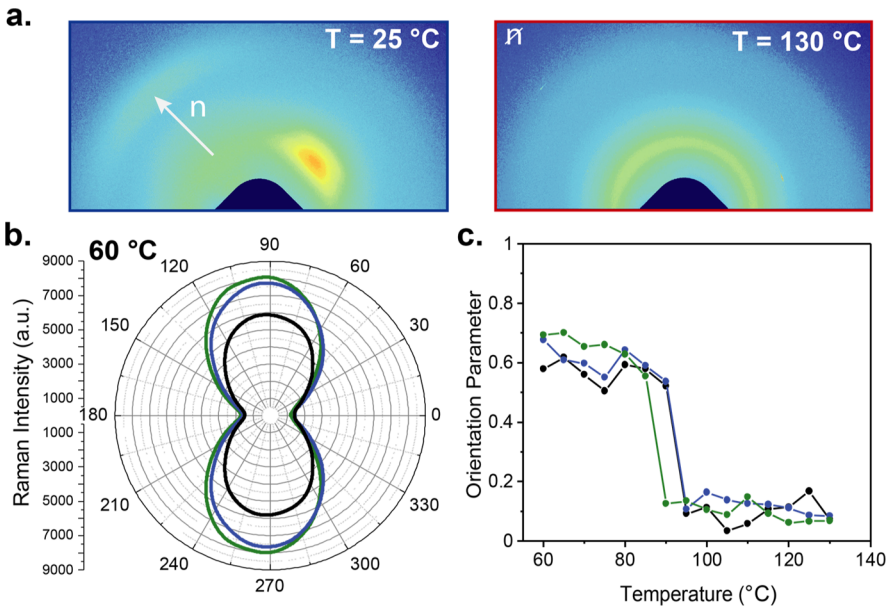

Figure 6. (a) WAXS patterns for C6M$_{0.6}$11OBA$_{0.4}$ are shown at room temperature and at 130 °C. (b) Polar graph of the 1606 cm^{-1} peak intensity illustrating well-aligned nematic LCEs at 60 °C as the laser polarization direction sweeps from 0 to 180°. (c) Plot of P2 (S) orientation parameter as a function of temperature calculated from polarized Raman data using two polarizers. C6M$_{1.0}$ (black), C6M$_{0.8}$11OBA$_{0.2}$ (blue), and C6M$_{0.6}$11OBA$_{0.4}$ (green).

We now further consider the thermomechanical response of the LCEs containing intra-mesogenic hydrogen bonds. The OBA dimers are similar in structure to a recent examination of LCEs prepared with biphenyl mesogens, which exhibit reduced mesogen−mesogen interactions that, accordingly, sharpen the stimuli response and shift it to lower temperatures.[26] To analyze the LCE thermotropic transition from nematic to isotropic for this system, WAXS was initially used, and the respective patterns show a considerable loss of order, as shown in Figures 6a and S13. Specifically, the orientation parameter (S) of the C6M$_{0.6}$11OBA$_{0.4}$ LCE goes from 0.79 to a value near zero, which corresponds to the associated thermomechanical response.

Additionally, we utilized Raman spectroscopy to monitor polarized orientation of phenyl rings during the phase transition of the LCE on heating. The LCEs were heated in 5 °C intervals between 60 and 130 °C with a 2 min equilibration at each temperature point. Following equilibration, a polarized Raman spectrum was collected using phase angles from 0 to 180°, which corresponds to the laser polarization angle (Figure S14). The change in Raman intensity for the 1606 cm^{-1} peak, the Raman shift for the uniaxial phenyl breathing mode, was plotted and is indicative of changes in alignment as a function of temperature and phase angle (Figures 6b and S15).[53] The hourglass shape of these measurements on the LCEs, with minimum peak intensity at 0 and 180° and maximum peak intensity at 90 and 270°, confirms anisotropy within the film (Figure 6b). The polar plots for each LCE as a function of temperature are presented in Figure S15, where the loss of order is evident in the transition from hourglass to circular plots. These experiments were then repeated using two polarizers oriented either parallel or perpendicular to each other, with one polarizing the incident laser beam before the sample and the other polarizer acting on the scattered light before the detector. Analysis of these data, which is detailed in the Supporting Information S16, yields an orientation parameter for the materials. Plotting the calculated orientation parameter against temperature illustrates the distinctive temperature dependence of the two OBA-containing LCEs (Figure 6c). LCEs prepared with increasing concentrations of 11OBA mesogens maintain higher orientation parameters in the monodomain state. The change in orientation parameter as a function of temperature mirrors the rate measurements in Figure 5a, with the change in orientation parameter first occurring in the C6M$_{0.6}$11OBA$_{0.4}$ LCE sample. Note that the temperature dependence of the Raman experiments and the mechanical measurements are shifted from one another, which may be attributable to experimental error. Ongoing experimentation is assessing the retention of paranematic orientation in the LCE, which will be complemented with advanced thermal analysis and spectroscopy study and detailed in a forthcoming report.

CONCLUSIONS

LCEs were prepared incorporating intra-mesogenic hydrogen-bonded dimers. The incorporation of supramolecular bonds affects the mechanical properties of these materials. Further, the mechanochemical nature of these bonds facilitates a distinctive method to align and realign these materials from the polydomain orientation. The thermomechanical response of the LCE shifts to lower temperatures and sharpens with increasing concentration of the supramolecular dimers in the materials. The actuation of the materials is clearly associated with the disruption of order in the LCE. Ongoing examination seeks to isolate the contribution of the temperature dependence of the hydrogen bonds on the thermomechanical response of these and related materials.

EXPERIMENTAL SECTION

Materials. All materials for LCE fabrication were purchased commercially and used as received. Components included 1,4-bis-[4-(6-acryloyloxyhexyloxy)benzoyloxy]-2-methylbenzene (C6M, Synthon Chemical), 4-(11-acryloylundecyloxyl) benzoic acid (11OBA, Synthon Chemical), 1,4-benzenedimethylthiol (BDMT, Sigma

https://doi.org/10.1021/acsami.2c18993
ACS Appl. Mater. Interfaces 2023, 15, 3467−3475

Aldrich), 4-methoxyphenol (MEHQ, Sigma-Aldrich), and bis(2,4,6-trimethylbenzoyl)phenylphosphine oxide (I-819, Omnirad).

LCE Fabrication. LC monomers C6M and 11OBA were combined with BDMT (0.9:1 molar ratio thiol:acrylate), radical inhibitor MEHQ (2 wt %), and photoinitiator I-819 (2 wt %). The solid powders were melted at 110 °C (isotropic temperature) using a heat gun and mixed thoroughly using a vortexer. The clear mixture was applied to a hot (110 °C on hot plate) Rain-X coated glass slide with 100 μm spacer strips. A second Rain-X coated slide was applied to the top of the mixture and secured using magnets. Kept at 110 °C, the full cell was exposed to UV light (365/405 nm, 10 mW cm^{-2}, 5 min per side). After exposure, the cell was cooled to room temperature and the polydomain film was removed.

LCE Alignment. Polydomain films were aligned either within the DMA (actuation experiments) or manually (Raman and X-ray experiments). For DMA studies, the films were heated to 90 °C, equilibrated at temperature, and then stretched into monodomain nematic at a rate of 5% min^{-1}. LCEs were stretched to 35, 120, or 150% strain for C6M$_{1.0}$, C6M$_{0.8}$11OBA$_{0.2}$, and C6M$_{0.6}$11OBA$_{0.4}$, respectively. The films were held at their final strain and cooled to room temperature, locking in nematic alignment. For nematic director realignment demonstrations, the LCEs were pulled to 70, 100, or 150% strain for C6M$_{1.0}$, C6M$_{0.8}$11OBA$_{0.2}$, and C6M$_{0.6}$11OBA$_{0.4}$, respectively, using calipers at room temperature and exposed to 90 °C heat with a heat gun. Upon cooling, the LCEs exhibited uniaxial nematic alignment with demonstrated birefringence. In both manual and automated alignment methods, LCEs were stretched to just before failure at the alignment temperature. The difference in the alignment strain values between the two methods is attributable to differences in the mechanical properties depending on the strain and heating rates.

Polarized Optical Microscopy. LCEs were analyzed using a Nikon Eclipse Ci-Pol microscope equipped with 5× and 10× objectives. Samples were imaged at 0 and 45° polarization angles to observe alignment. Phase transitions of the LCEs were observed using a heat stage heated from room temperature to 150 °C and images were correlated with DSC thermograms.

Dynamic Mechanical Analysis. Uniaxial tensile studies were performed using a TA Instruments RSA-G2 Dynamic Solids Analyzer. Polydomain LCEs were cut into rectangular strips (ca. 10 mm × 2 mm × 0.1 mm), loaded with a gap of ca. 5 mm, and strained at a rate of 5% min^{-1} at room temperature. Actuation studies were carried out using a TA Instruments Discovery 850 DMA equipped with a liquid nitrogen cooling system. Polydomain LCEs were cut into strips (ca. 10 mm × 2 mm × 0.1 mm) and loaded with a gap of ca. 5 mm. Samples were aligned in the DMA (see above LCE Alignment) and then subject to heat/cool/heat/cool (150/60/150/60 °C) cycles at a rate of 5 °C min^{-1} with a 2 min equilibration at each end temperature.

Attenuated Total Reflectance Infrared Spectroscopy. Attenuated total reflectance infrared spectroscopy (ATR-IR) studies were carried out using a Nicolet iS50 infrared spectrometer equipped with an ITO heating plate. For temperature-dependent studies, samples were placed over the ATR crystal and the heating plate was secured on top of the sample. Samples were heated from 50 to 150 °C at 5 °C intervals with 1 min equilibration times at each temperature point. Spectra were collected with 32 scans at a resolution of 4 cm^{-1} in the range of 4000 to 525 cm^{-1}.

Polarized Raman Spectroscopy. Raman spectra were collected using a Horiba LabRAM HR Evolution Raman spectrometer at the Raman Microspectroscopy Laboratory at the University of Colorado-Boulder (RRID: SCR_019305). The 532 nm laser beam was focused through a 100× objective lens and attenuated to 25% of the power at the source. The spectrometer was calibrated using the 520 cm^{-1} Raman peak of Si prior to analysis. Spectra were then collected from 100 to 2000 cm^{-1} using a 600 lines mm^{-1} grating. The polarization direction of the excitation laser was controlled using a motorized half-wave plate. An ITO heating plate was used to heat each sample from 60 to 130 °C at 5 °C intervals with 2 min equilibration times at each temperature point. Temperature-dependent studies were implemented by placing a monodomain sample (see above LCE Alignment) on the heating plate and focusing the Raman laser beam on the material. At each temperature, the laser polarization direction was rotated from 0 to 180° by 10° steps relative to the sample's nematic director. For the experiments used to find the orientation parameter, the Raman scattered light was additionally passed through a motorized polarizing filter (analyzer), which was oriented either parallel or perpendicular to the laser polarization direction and then through a depolarizer before the spectrometer. Spectra were collected by averaging two spectra collected with a 15 s counting time each. Spectra were processed using LabSpec 6 software (Horiba Scientific), including subtraction of a polynomial baseline fit.

Wide Angle X-ray Scattering. Static WAXS experiments were collected on beamline 11-BM Complex Materials Scattering (CMS) at the National Synchrotron Light Source-II (NSLS-II) at Brookhaven National Laboratory and 5-ID-B,C,D at the Advanced Photon Source (APS) at Argonne National Laboratory. Patterns were acquired on samples using X-rays with 13.5 keV energy and 10 s exposures at NSLS-II and X-rays with 17 keV energy at APS with 5 s exposures. Heat treatments were performed on beamline supplied Linkam Thermal Stages (Linkam THMS600 and Link\APS and NSLS-II, respectively). Patterns were collected at various temperatures approximately every 5 °C between 60 and 130 °C with room temperature scans collected initially. Temperature-dependent studies were implemented with a monodomain sample (see above LCE Alignment). Data reduction and orientation parameter calculations were performed in Igor using the Nika analytical package and through a custom script in MATLAB (Version R2021b), respectively.[54]

■ ASSOCIATED CONTENT

Supporting Information

The Supporting Information is available free of charge at https://pubs.acs.org/doi/10.1021/acsami.2c18993.

DSC traces, cross polarized images of aligned films, WAXS patterns, demo photos, IR spectra, actuation data, Raman spectra, and order parameter calculation (PDF)

■ AUTHOR INFORMATION

Corresponding Author

Timothy J. White − *Department of Chemical and Biological Engineering and Material Science and Engineering Program, University of Colorado Boulder, Boulder, Colorado 80309, United States;* orcid.org/0000-0001-8006-7173; Email: timothy.j.white@colorado.edu

Authors

Kristin L. Lewis − *Department of Chemical and Biological Engineering, University of Colorado Boulder, Boulder, Colorado 80309, United States;* orcid.org/0000-0003-1897-2855

Katie M. Herbert − *Department of Chemical and Biological Engineering, University of Colorado Boulder, Boulder, Colorado 80309, United States*

Valentina M. Matavulj − *Material Science and Engineering Program, University of Colorado Boulder, Boulder, Colorado 80309, United States*

Jonathan D. Hoang − *Material Science and Engineering Program, University of Colorado Boulder, Boulder, Colorado 80309, United States*

Eric T. Ellison − *Department of Geological Sciences, University of Colorado Boulder, Boulder, Colorado 80309, United States*

Grant E. Bauman − *Department of Chemical and Biological Engineering, University of Colorado Boulder, Boulder, Colorado 80309, United States*

Jeremy A. Herman − *Department of Chemical and Biological Engineering, University of Colorado Boulder, Boulder, Colorado 80309, United States*

Complete contact information is available at: https://pubs.acs.org/10.1021/acsami.2c18993

Author Contributions

‖K.L.L. and K.M.H. contributed significantly to this work. The manuscript was written through contributions of all authors. All authors have given approval to the final version of the manuscript.

Funding

The authors acknowledge financial support from the Army Research Office, the U.S. Air Force, the National Science Foundation (DMR 2105369, GRF to J.A.H.), the Department of Education through the GAANN Fellowship (K.L.L.), and the Department of Defense through the NDSEG Fellowship (K.L.L., G.E.B.).

Notes

The authors declare no competing financial interest.

■ ACKNOWLEDGMENTS

This research used data collected at 11-BM CMS of the National Synchrotron Light Source II, a U.S. Department of Energy (DOE) Office of Science User Facility operated for the DOE Office of Science by Brookhaven National Laboratory under contract no. DE-SC0012704. Portions of this work were performed at the DuPont-Northwestern-Dow Collaborative Access Team (DND-CAT) located at Sector 5 of the Advanced Photon Source (APS). DND-CAT is supported by Northwestern University, The Dow Chemical Company, and DuPont de Nemours, Inc. This research used resources of the Advanced Photon Source, a U.S. Department of Energy (DOE) Office of Science User Facility operated for the DOE Office of Science by Argonne National Laboratory under contract no. DE-AC02-06CH11357. Data was collected using an instrument funded by the National Science Foundation under Award no 0960140.

■ ABBREVIATIONS

LC, liquid crystal
LCE, liquid crystalline elastomer
DSC, differential scanning calorimetry
POM, polarized optical microscopy
WAXS, wide angle X-ray scattering
ATR, attenuated total reflectance infrared spectroscopy
DMA, dynamic mechanical analysis

■ REFERENCES

(1) López-Valdeolivas, M.; Liu, D.; Broer, D. J.; Sánchez-Somolinos, C. 4D Printed Actuators with Soft-Robotic Functions. *Macromol. Rapid Commun.* **2018**, *39*, 1700710.
(2) Wang, Z.; Li, K.; He, Q.; Cai, S. A Light-Powered Ultralight Tensegrity Robot with High Deformability and Load Capacity. *Adv. Mater.* **2019**, *31*, 1806849.
(3) Kotikian, A.; McMahan, C.; Davidson, E. C.; Muhammad, J. M.; Weeks, R. D.; Daraio, C.; Lewis, J. A. Untethered Soft Robotic Matter with Passive Control of Shape Morphing and Propulsion. *Sci. Rob.* **2019**, *4*, No. eaax7044.
(4) Jiang, J.; Dhakal, N. P.; Guo, Y.; Andre, C.; Thompson, L.; Skalli, O.; Peng, C. Controlled Dynamics of Neural Tumor Cells by Templated Liquid Crystalline Polymer Networks. *Adv. Healthcare Mater.* **2020**, *9*, 2000487.
(5) Prévôt, M. E.; Andro, H.; Alexander, S. L. M.; Ustunel, S.; Zhu, C.; Nikolov, Z.; Rafferty, S. T.; Brannum, M. T.; Kinsel, B.; Korley, L. T. J.; Freeman, E. J.; McDonough, J. A.; Clements, R. J.; Hegmann, E. Liquid Crystal Elastomer Foams with Elastic Properties Specifically Engineered as Biodegradable Brain Tissue Scaffolds. *Soft Matter* **2018**, *14*, 354−360.
(6) Stumpel, J. E.; Wouters, C.; Herzer, N.; Ziegler, J.; Broer, D. J.; Bastiaansen, C. W. M.; Schenning, A. P. H. J. An Optical Sensor for Volatile Amines Based on an Inkjet-Printed, Hydrogen-Bonded, Cholesteric Liquid Crystalline Film. *Adv. Opt. Mater.* **2014**, *2*, 459−464.
(7) Brannum, M. T.; Steele, A. M.; Venetos, M. C.; Korley, L. S. T. J.; Wnek, G. E.; White, T. J. Light Control with Liquid Crystalline Elastomers. *Adv. Opt. Mater.* **2019**, *7*, 1801683.
(8) Winkler, M.; Kaiser, A.; Krause, S.; Finkelmann, H.; Schmidt, A. M. Liquid Crystal Elastomers with Magnetic Actuation. *Macromol. Symp.* **2010**, *291*−*292*, 186−192.
(9) Ware, T. H. H.; White, T. J. J. Programmed Liquid Crystal Elastomers with Tunable Actuation Strain. *Polym. Chem.* **2015**, *6*, 4835−4844.
(10) Roach, D. J.; Yuan, C.; Kuang, X.; Li, V. C. F.; Blake, P.; Romero, M. L.; Hammel, I.; Yu, K.; Qi, H. J. Long Liquid Crystal Elastomer Fibers with Large Reversible Actuation Strains for Smart Textiles and Artificial Muscles. *ACS Appl. Mater. Interfaces* **2019**, *11*, 19514−19521.
(11) McCracken, J. M.; Donovan, B. R.; White, T. J. Materials as Machines. *Adv. Mater.* **2020**, *32*, 1906564.
(12) Martella, D.; Parmeggiani, C. Advances in Cell Scaffolds for Tissue Engineering: The Value of Liquid Crystalline Elastomers. *Chem.—Eur. J.* **2018**, *24*, 12206−12220.
(13) Babakhanova, G.; Krieger, J.; Li, B. X.; Turiv, T.; Kim, M. H.; Lavrentovich, O. D. Cell Alignment by Smectic Liquid Crystal Elastomer Coatings with Nanogrooves. *J. Biomed. Mater. Res., Part A* **2020**, *108*, 1223−1230.
(14) Prévôt, M. E.; Bergquist, L. E.; Sharma, A.; Mori, T.; Gao, Y.; Bera, T.; Zhu, C.; Leslie, M. T.; Cukelj, R.; Korley, L. T.; Freeman, E. J.; McDonough, J. A.; Clements, R. J.; Hegmann, E.New Developments in 3D Liquid Crystal Elastomers Scaffolds for Tissue Engineering: From Physical Template to Responsive Substrate. In *Liquid Crystals XXI*; Khoo, I. C., Ed.; SPIE, 2017; p 28.
(15) Broer, D. J.; Lub, J.; Mol, G. N. Wide-Band Reflective Polarizers from Cholesteric Polymer Networks with a Pitch Gradient. *Nature* **1995**, *378*, 467−469.
(16) Wermter, H.; Finkelmann, H. Liquid Crystalline Elastomers as Artificial Muscles. *e-Polymers* **2001**, *1*, 111.
(17) Yakacki, C. M.; Saed, M.; Nair, D. P.; Gong, T.; Reed, S. M.; Bowman, C. N. Tailorable and Programmable Liquid-Crystalline Elastomers Using a Two-Stage Thiol-Acrylate Reaction. *RSC Adv.* **2015**, *5*, 18997−19001.
(18) Herbert, K. M.; Fowler, H. E.; McCracken, J. M.; Schlafmann, K. R.; Koch, J. A.; White, T. J. Synthesis and Alignment of Liquid Crystalline Elastomers. *Nat. Rev. Mater.* **2022**, *7*, 23−38.
(19) Ware, T. H.; McConney, M. E.; Wie, J. J.; Tondiglia, V. P.; White, T. J. Voxelated Liquid Crystal Elastomers. *Science* **2015**, *347*, 982−984.
(20) Jiang, L.; Huang, W.; Xue, X.; Yang, H.; Jiang, B.; Zhang, D.; Fang, J.; Chen, J.; Yang, Y.; Zhai, G.; Kong, L.; Wang, S. Radical Polymerization in the Presence of Chain Transfer Monomer: An Approach to Branched Vinyl Polymers. *Macromolecules* **2012**, *45*, 4092−4100.
(21) Ware, T. H.; Perry, Z. P.; Middleton, C. M.; Iacono, S. T.; White, T. J. Programmable Liquid Crystal Elastomers Prepared by Thiol-Ene Photopolymerization. *ACS Macro Lett.* **2015**, *4*, 942−946.
(22) Küpfer, J.; Finkelmann, H. Nematic Liquid Single Crystal Elastomers. *Makromol. Chem. Rapid Commun.* **1991**, *12*, 717−726.
(23) Brannum, M. T.; Auguste, A. D.; Donovan, B. R.; Godman, N. P.; Matavulj, V. M.; Steele, A. M.; Korley, L. S. T. J.; Wnek, G. E.; White, T. J. Deformation and Elastic Recovery of Acrylate-Based Liquid Crystalline Elastomers. *Macromolecules* **2019**, *52*, 8248−8255.

(24) Godman, N. P.; Kowalski, B. A.; Auguste, A. D.; Koerner, H.; White, T. J. Synthesis of Elastomeric Liquid Crystalline Polymer Networks via Chain Transfer. *ACS Macro Lett.* **2017**, *6*, 1290−1295.
(25) Hebner, T. S.; Fowler, H. E.; Herbert, K. M.; Skillin, N. P.; Bowman, C. N.; White, T. J. Polymer Network Structure, Properties, and Formation of Liquid Crystalline Elastomers Prepared via Thiol−Acrylate Chain Transfer Reactions. *Macromolecules* **2021**, *54*, 11074−11082.
(26) McCracken, J. M.; Donovan, B. R.; Lynch, K. M.; White, T. J. Molecular Engineering of Mesogenic Constituents Within Liquid Crystalline Elastomers to Sharpen Thermotropic Actuation. *Adv. Funct. Mater.* **2021**, *31*, 2100564.
(27) Lee, Y.; Choi, S.; Kang, B.-G.; Ahn, S.-K. Effect of Isomeric Amine Chain Extenders and Crosslink Density on the Properties of Liquid Crystal Elastomers. *Materials* **2020**, *13*, 3094.
(28) Saed, M. O.; Ambulo, C. P.; Kim, H.; De, R.; Raval, V.; Searles, K.; Siddiqui, D. A.; Cue, J. M. O.; Stefan, M. C.; Shankar, M. R.; Ware, T. H. Molecularly-Engineered, 4D-Printed Liquid Crystal Elastomer Actuators. *Adv. Funct. Mater.* **2019**, *29*, 1806412.
(29) Saed, M. O.; Gablier, A.; Terentjev, E. M. Exchangeable Liquid Crystalline Elastomers and Their Applications. *Chem. Rev.* **2022**, *122*, 4927−4945.
(30) Lee, J.; Bae, J.; Hwang, J. H.; Choi, M.; Kim, Y. S.; Park, S.; Na, J.; Kim, D.; Ahn, S. Robust and Reprocessable Artificial Muscles Based on Liquid Crystal Elastomers with Dynamic Thiourea Bonds. *Adv. Funct. Mater.* **2022**, *32*, 2110360.
(31) Wang, Z.; Tian, H.; He, Q.; Cai, S. Reprogrammable, Reprocessible, and Self-Healable Liquid Crystal Elastomer with Exchangeable Disulfide Bonds. *ACS Appl. Mater. Interfaces* **2017**, *9*, 33119−33128.
(32) Pei, Z.; Yang, Y.; Chen, Q.; Terentjev, E. M.; Wei, Y.; Ji, Y. Mouldable Liquid-Crystalline Elastomer Actuators with Exchangeable Covalent Bonds. *Nat. Mater.* **2014**, *13*, 36−41.
(33) Saed, M. O.; Terentjev, E. M. Siloxane Crosslinks with Dynamic Bond Exchange Enable Shape Programming in Liquid-Crystalline Elastomers. *Sci. Rep.* **2020**, *10*, 6609.
(34) Wang, Z.; He, Q.; Wang, Y.; Cai, S. Programmable Actuation of Liquid Crystal Elastomers: Via "Living" Exchange Reaction. *Soft Matter* **2019**, *15*, 2811−2816.
(35) McBride, M. K.; Martinez, A. M.; Cox, L.; Alim, M.; Childress, K.; Beiswinger, M.; Podgorski, M.; Worrell, B. T.; Killgore, J.; Bowman, C. N. A Readily Programmable, Fully Reversible Shape-Switching Material. *Sci. Adv.* **2018**, *4*, No. eaat4634.
(36) Ni, B.; Xie, H.; Tang, J.; Zhang, H. L.; Chen, E. Q. A Self-Healing Photoinduced-Deformable Material Fabricated by Liquid Crystalline Elastomers Using Multivalent Hydrogen Bonds as Cross-Linkers. *Chem. Commun.* **2016**, *52*, 10257−10260.
(37) Li, M.; Dai, S.; Dong, X.; Jiang, Y.; Ge, J.; Xu, Y.; Yuan, N.; Ding, J. High-Strength, Large-Deformation, Dual Cross-Linking Network Liquid Crystal Elastomers Based on Quadruple Hydrogen Bonds. *Langmuir* **2022**, *38*, 1560−1566.
(38) Lugger, S. J. D.; Mulder, D. J.; Schenning, A. P. H. J. One-Pot Synthesis of Melt-Processable Supramolecular Soft Actuators. *Angew. Chem., Int. Ed.* **2022**, *61*, No. e202115166.
(39) Lugger, S. J. D.; Verbroekken, R. M. C.; Mulder, D. J.; Schenning, A. P. H. J. Direct Ink Writing of Recyclable Supramolecular Soft Actuators. *ACS Macro Lett.* **2022**, *11*, 935−940.
(40) Lugger, S. J. D.; Houben, S. J. A.; Foelen, Y.; Debije, M. G.; Schenning, A. P. H. J.; Mulder, D. J. Hydrogen-Bonded Supramolecular Liquid Crystal Polymers: Smart Materials with Stimuli-Responsive, Self-Healing, and Recyclable Properties. *Chem. Rev.* **2022**, *122*, 4946−4975.
(41) Houben, S. J. A.; Lugger, S. J. D.; van Raak, R. J. H.; Schenning, A. P. H. J. A PH-Responsive Liquid Crystal Hydrogel Actuator with Calcium-Induced Reprogrammable Shape Fixing. *ACS Appl. Polym. Mater.* **2022**, *4*, 1298−1304.
(42) Abadia, A. V.; Herbert, K. M.; White, T. J.; Schwartz, D. K.; Kaar, J. L. Biocatalytic 3D Actuation in Liquid Crystal Elastomers via Enzyme Patterning. *ACS Appl. Mater. Interfaces* **2022**, *14*, 26480−26488.
(43) Velasco Abadia, A.; Herbert, K. M.; Matavulj, V. M.; White, T. J.; Schwartz, D. K.; Kaar, J. L. Chemically Triggered Changes in Mechanical Properties of Responsive Liquid Crystal Polymer Networks with Immobilized Urease. *J. Am. Chem. Soc.* **2021**, *143*, 16740−16749.
(44) Li, Y.; Zhuo, H.; Chen, H.; Chen, S. Novel Photo-Thermal Staged-Responsive Supramolecular Shape Memory Polyurethane Complex. *Polymer* **2019**, *179*, 121671.
(45) Kato, T.; Frechet, J. M. J.; Wilson, P. G.; Saito, T.; Uryu, T.; Fujishima, A.; Jin, C.; Kaneuchi, F. Hydrogen-Bonded Liquid Crystals. Novel Mesogens Incorporating Nonmesogenic Bipyridyl Compounds through Complexation between H-Bond Donor and Acceptor Moieties. *Chem. Mater.* **1993**, *5*, 1094−1100.
(46) Broer, D. J.; Bastiaansen, C. M. W.; Debije, M. G.; Schenning, A. P. H. J. Functional Organic Materials Based on Polymerized Liquid-Crystal Monomers: Supramolecular Hydrogen-Bonded Systems. *Angew. Chem., Int. Ed.* **2012**, *51*, 7102−7109.
(47) Shandryuk, G. A.; Kuptsov, S. A.; Shatalova, A. M.; Plate, N. A.; Talroze, R. V. Liquid Crystal H-Bonded Polymer Networks under Mechanical Stress. *Macromolecules* **2003**, *36*, 3417−3423.
(48) Kato, T.; Jin, C.; Kaneuchi, F.; Uryu, T.*Effect of the Molecular Orientation on the Stability of Hydrogen-Bonded Benzoic Acid Dimers. Infrared Study of Liquid-Crystalline 4-Alkylbenzoic Acids*; Bulletin of the Chemical Society of Japan, 1993; Vol. *66*, pp 3581−3584.
(49) Warner, M.; Bladon, P.; Terentjev, E. M. "Soft Elasticity" — Deformation without Resistance in Liquid Crystal Elastomers. *J. Phys. II* **1994**, *4*, 93−102.
(50) Warner, M.; Terentjev, E. M.*Liquid Crystal Elastomers*; Oxford Science Publications, 2019; Vol. *53*.
(51) Kato, T.; Fréchet, J. M. J.; Uryu, T.; Kaneuchi, F.; Jin, C.; Fréchet, J. M. J. Hydrogen-bonded Liquid Crystals Built from Hydrogen-bonding Donors and Acceptors Infrared Study on the Stability of the Hydrogen Bond between Carboxylic Acid and Pyridyl Moieties. *Liq. Cryst.* **2006**, *33*, 1429−1437.
(52) Martínez-Felipe, A.; Imrie, C. T. The Role of Hydrogen Bonding in the Phase Behaviour of Supramolecular Liquid Crystal Dimers. *J. Mol. Struct.* **2015**, *1100*, 429−437.
(53) Southern, C. D.; Gleeson, H. F. Using the Full Raman Depolarisation in the Determination of the Order Parameters in Liquid Crystal Systems. *Eur. Phys. J. E: Soft Matter Biol. Phys.* **2007**, *24*, 119−127.
(54) Ilavsky, J. Nika : Software for Two-Dimensional Data Reduction. *J. Appl. Crystallogr.* **2012**, *45*, 324−328.

https://doi.org/10.1021/acsami.2c18993
ACS Appl. Mater. Interfaces 2023, 15, 3467−3475